Chemical Science

EDGE ARTICLE

Electronically and geometrically complementary perylenediimides for kinetically controlled supramolecular copolymers†

Alfonso J. Schwalb, Fátima García and Luis Sánchez [ID] *

The synthesis of 3,4,9,10-benzo[*d,e*]isoquinolino[1,8-*g,h*]quinoline-tetracarboxylic diimide (BQQDI) **1** endowed with peripheral trialkoxybenzamide fragments is reported and its self-assembling features investigated. The peripheral benzamide moieties generate metastable monomeric species that afford a kinetically controlled supramolecular polymerization. The electron-withdrawing character of **1** in comparison with previously reported PDIs **2**, together with the similar geometry, makes this dye an optimal candidate to perform seeded supramolecular copolymerization yielding four different supramolecular block copolymers. Whilst heteropolymers **poly-1-co-2a**, **poly-2a-co-1** and **poly-1-co-2b** present an H-type arrangement of the monomeric units, heteropolymer **poly-2b-co-1**, prepared by seeding the chiral, metastable monomers of **2b** with achiral seeds of **1**, produces chiral, J-type aggregates. Interestingly, the monosignated CD signal of pristine **poly-2b** changes to a bisignated CD signal most probably due to the formation of columnar domains around the seeds of **1** which implies the blocky nature of the supramolecular copolymers formed.

Introduction

Natural coassembly, a process by which different elements come together spontaneously to form a complex structure, is ubiquitous in life sciences. Cell membranes, in which lipids, proteins and some other molecules form a functional bilayer structure, are remarkable examples of biological coassembly.[1] Regarding chemical coassembled systems, block copolymers are exciting examples, which are constituted by covalently linked immiscible homopolymer blocks that give rise to well defined nanostructures, holding applicability in different areas like drug delivery, coatings, adhesives, and as templates for the synthesis of nanomaterials. In these block copolymers, as in the case of conventional polymers, the junction between the monomeric units are covalent bonds.[2] In the last decades, a number of supramolecular polymers, *i.e.*, macromolecules in which the monomeric units are held together by non-covalent interactions,[3] has arisen as functional materials finding out applicability as biomaterials,[4] elastomers,[5] photocatalysts,[6] adhesives,[7] self-healing materials,[8] or as active layer in optoelectronic devices.[9] The development of supramolecular polymers relies, among some other factors, on the reported mass-balance model that allows deriving a complete set of

thermodynamic parameters associated to the supramolecular polymerization process.[10]

Despite a large number of supramolecular polymers are thermodynamically controlled and governed by an isodesmic or a cooperative (or nucleation–elongation) mechanism,[3] the last years have witnessed the growth of kinetically controlled supramolecular polymerizations in which the self-assembly is retarded. In these kinetically controlled examples, competitive or consecutive processes yielding different supramolecular aggregated species can take place.[3b,11] Furthermore, in good analogy with living crystallization driven self-assembly reported for covalent block copolymers,[12] kinetically controlled processes have been utilized to perform living (LSP) and seeded (SSP) supramolecular polymerizations that decreases the polydispersity in the supramolecular polymers.[13]

Both thermodynamically and kinetically controlled supramolecular polymerizations have been harnessed to prepare supramolecular block copolymers (SBCPs) in which two or more different monomeric species non-covalently bonded yield new adaptive and functional materials.[14] A key issue in the further development of block supramolecular polymers is controlling the microstructure (self-sorted, block, blocky, periodic, statistical or alternated) of the final coassembled species. In thermodynamically controlled supramolecular copolymers, it is difficult to control such microstructure but the recently reported mass-balance model reported by ten Eikelder and coworkers[15] has allowed to unravel the microstructure of thermodynamically controlled heteropolymers once they are formed.[16] On the other hand, kinetically controlled

Departamento de Química Orgánica, Facultad de Ciencias Químicas, Universidad Complutense de Madrid, 28040 Madrid, Spain. E-mail: lusamar@ucm.es

† Electronic supplementary information (ESI) available. See DOI: https://doi.org/10.1039/d4sc01322k

supramolecular copolymerizations have been reported to yield alternating supramolecular copolymers. The sequential addition of metastable monomers, able to undergo nucleation–elongation growth, is crucial to produce seeded supramolecular copolymerizations affording such alternating coassemblies. An elegant example of kinetically controlled SBCPs is that reported by Sugiyasu and co-workers based on Zn and Cu porphyrins in which while the Zn-core homopolymer is unstable, the heteropolymer constituted by fragments of both the Zn and the Cu-core porphyrins presents an enhanced stability.[17] Another example of kinetically controlled SBCPs is the stereoselective coassembly of two napthalendiimides with the same point chirality at the binaphtyl-based linker and with electronically complementary character.[18] Of special interest due to their intriguing characteristics and applications,[19] is the kinetically controlled coassembly of electronically complementary perylenediimides (PDIs) described by F. Würthner and coworkers to form $(A_nBB)_m$ alternating species.[20] Kinetically controlled coassembly allows for the deliberate design and control of the assembly process, influencing the structures and properties of the resulting supramolecular polymers and, hence, new insights into the requirements to achieve SBCPs with controlled microstructure are necessary.

Herein, we envision that 3,4,9,10-benzo[d,e]isoquinolino[1,8-g,h]quinolinetetracarboxylic diimide (BQQDI)[21] could be an excellent complementary scaffold to perform a seeded supramolecular copolymerization with previously reported PDIs **2** due to its enhanced electron-withdrawing character. Thus, we have synthesized the BQQDI **1** endowed with peripheral trialkoxybenzamide fragments (Fig. 1a). The π-surface of the BQQDI **1** together with the benzamide units allows its efficient supramolecular polymerization, governed by a cooperative mechanism, to afford H-type aggregates. At the same time, this peripheral benzamide groups provoke the formation of metastable monomeric species, M^*, that retards the self-assembly of **1** to form the homopolymer **poly-1**. The autocatalytic time-dependent growth of **1** homopolymers can be accelerated by adding seeds. As stated before, the electron-withdrawing features of **1** together with its planar geometry makes this BQQDI an excellent scaffold to prepare kinetically controlled SBCPs with previously reported PDIs **2a** and **2b**, due to their geometric and electronic complementarity (Fig. 1a).[13c,22] Whilst achiral **2a** has been reported to form kinetically controlled H-type aggregates (**poly-2a**),[13c] chiral **2b** yields J-type aggregated species (**poly-2b**) upon self-assembly (Fig. 1b).[22a,22b] Harnessing the dissimilar self-assembling features of the PDIs **2** and by using a SSP strategy, we have been able to prepare **poly-1-co-2a**, **poly-1-co-2b**, **poly-2a-co-1** and **poly-2b-co-1** supramolecular block copolymers of tailored H- or J-type character, thus shedding new insights to achieve electroactive heteropolymers (Fig. 1c).

Results and discussion

Synthesis and homopolymerization of BQQDI 1

The synthesis of BQQDI **1** has been accomplished by following a convergent strategy in which dianhydride **9** was prepared by following the multistep protocol reported by Okamoto *et al.* in 2020.[21a] The synthesis starts with two aromatic nucleophilic substitutions in 1,5-dinitroanthraquinone followed by condensation in acidic conditions that yields diester **4** with nitrogen doped perylene scaffold present in target BQQDI **1**. Treatment of **4** with *N*-phenyl-bis(trifluoromethanesulfonimide), followed by reduction with formic acid, bromination with NBS, Pd(0)
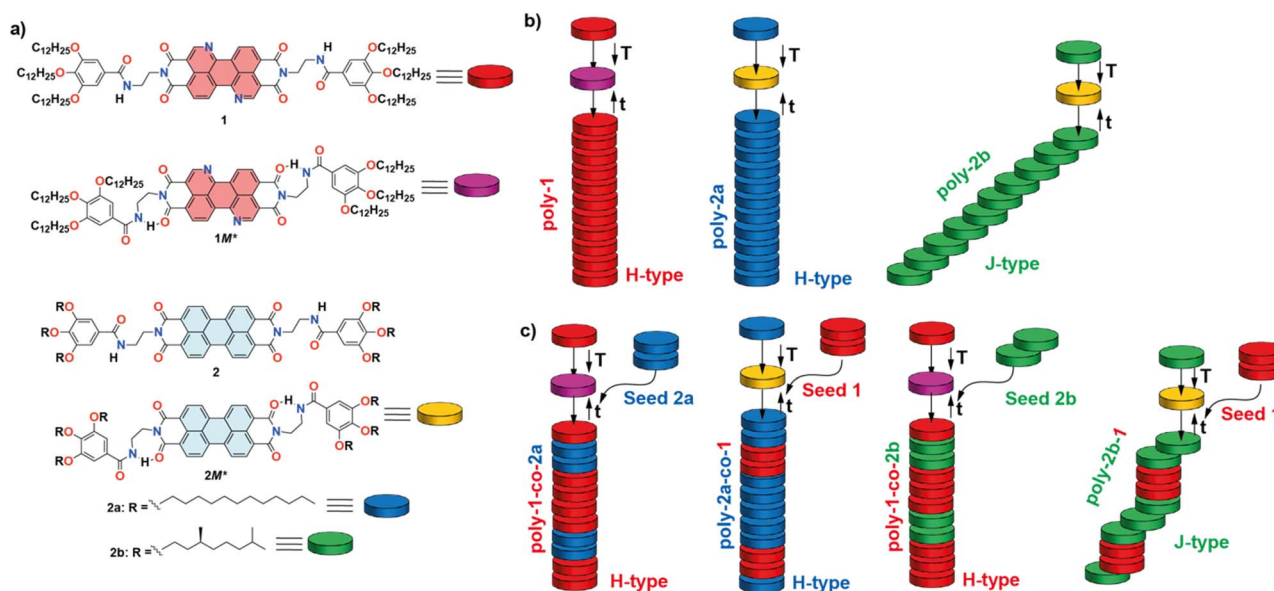

Fig. 1 (a) Chemical structure of BQQDI **1** and the electronically and geometrically complementary PDIs **2** depicting the chemical structure of the intramolecularly H-bonded pseudocycles (*M**); (b) schematic representation of the formation of kinetically controlled homopolymers **poly-1**, **poly-2a** and **poly-2b** through the metastable monomeric species *M**; (c) schematic illustration of the seeded supramolecular polymerization yielding heteropolymers **poly-1-co-2a**, **poly-2a-co-1**, **poly-1-2b** and **poly-2b-co-1**.

coupling and treatment with *p*-TsOH at high temperatures yields dianhydride **9** (see Scheme S1 in ESI†).[21a] On the other hand, the peripheral benzamide moiety was prepared by following previously reported protocols.[22] Finally, a two-fold condensation reaction under microwave irradiation between dianhydride **9** and benzamide **10** in the presence of propionic acid and *o*-dichlorobenzene as solvent yields BQQDI **1** in 21% yield (Scheme S1†). The chemical structure of the BQQDI **1** has been elucidated by the standard techniques (see ESI†).

The self-assembling features of **1** in solution have been investigated by different spectroscopic techniques. To our surprise, **1** is sparingly soluble in most common organic solvents at relatively high concentrations. In fact, BQQDI **1** in CDCl$_3$ at total concentration (c_T) above 10 mM precipitates which impedes performing concentration dependent ^{1}H NMR experiments that could contribute to clarify the non-covalent forces involved in the supramolecular polymerization. However, heating up a solution of **1** in CDCl$_3$ at $c_T = 4$ mM shows that, whilst the aromatic protons shield moderately upon decreasing the temperature, the opposite effect is observed for the amide protons. This is indicative of the π-stacking of the aromatic backbones and the formation of intermolecular H-bonding interactions between the amide groups, respectively (Fig. S1†). FTIR in solution has been utilized to demonstrate the formation of intermolecular H-bonds between the amide functional groups in non-polar solvents like methylcyclohexane (MCH). The stretching NH and amide I bands of **1** in MCH appears at 3260 and 1636 cm^{-1}, respectively (Fig. 2a). These values are ascribable to the formation of intermolecular H-bonded amides.[23] In CHCl$_3$, a good solvent that favors the complete solvation of the monomeric species, two stretching NH bands centered at 3454 and 3414 cm^{-1} are observed, ascribable to free NH and intramolecular NH H-bonds, due to the presence of completely free monomeric species and seven-membered H-bonded pseudocycles formed by the intramolecular interaction between the NH of the amide groups and one of the carbonyls of the imide moiety (Fig. 1a and 2a).[23] The formation of these pseudocycles has been corroborated by

registering ^{1}H NMR spectra at $c_T = 1$ mM and at different temperatures. In these experiments, unlike in the previous studies carried out a 4 mM, none of the resonances corresponding to the aromatic protons experience any shift upon modifying the temperature. However, the triplet corresponding to the NH proton shifts upfield upon increasing the temperature, diagnostic of the rupture of the intramolecular H-bonding interactions (Fig. 2b). The formation of such metastable monomeric species has been reported to provoke kinetically controlled supramolecular polymerizations.[23] In fact, variable temperature (VT) UV-Vis studies confirm that these dormant species retard the formation of the homopolymers **poly-1**.

In an attempt to derive the thermodynamic parameters associated to the supramolecular polymerization of **1**, we first utilized diluted solutions of **1** in MCH. In pristine MCH, the UV-Vis spectrum of BQQDI **1** at 20 °C shows maxima centered at $\lambda = 469$, 503 and 536 nm. These absorption bands are less intense than those observed in CHCl$_3$ with maxima centered at $\lambda = 454$, 485 and 520 nm, ascribable to the characteristic A$_{0-1}$/A$_{0-0}$- transitions of pyrene-based scaffolds (Fig. S2†).[19] These changes observed in the UV-Vis spectra implies the H-type nature of the supramolecular polymers formed by **1** in which the monomeric units are arranged in a face-to-face fashion. The UV-Vis spectrum of **1** in MCH upon heating up the solution at 90 °C does not match with that registered in CHCl$_3$ and ascribable to the monomeric species. Therefore, only a partial disassembly of the H-type aggregates formed at low temperatures is achieved by heating up this MCH solution (Fig. S2b†). To decrease the stability of the supramolecular polymers formed by **1**, we have utilized toluene (Tol) as solvent. In this case, the UV-Vis solution in Tol at 20 °C displays an identical absorption pattern to that registered in MCH at 20 °C diagnostic of the formation of the H-type aggregates (Fig. 3a). Heating up the Tol solution of **1** to 90 °C provokes a complete disassembly of these aggregated species, as demonstrate the UV-Vis absorption pattern coincident with that registered in CHCl$_3$ (Fig. 3a and S2b†). Plotting the variation of the absorbance at $\lambda = 520$ nm against temperature upon cooling at 1 °C min^{-1} yields a non-sigmoidal curve that could be
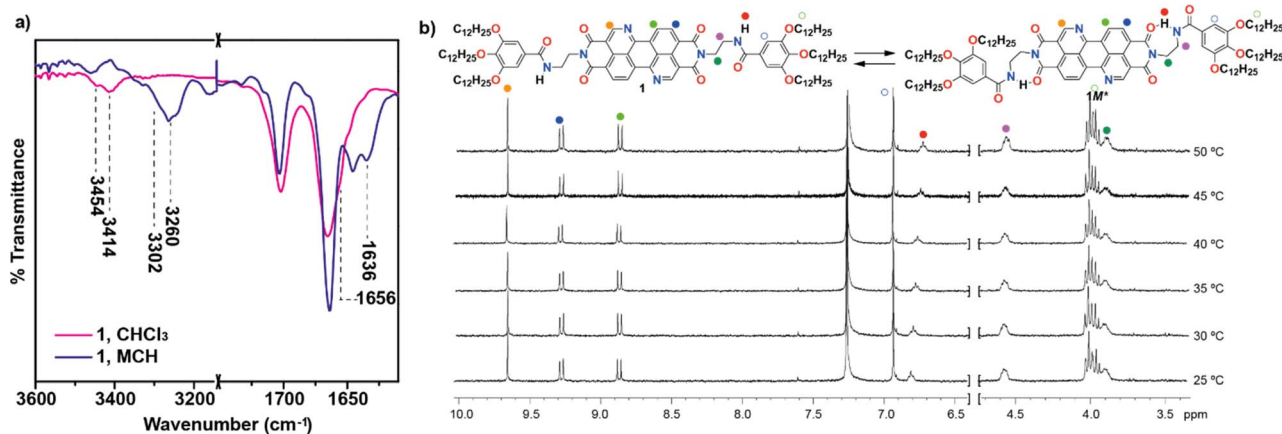

Fig. 2 (a) Partial FTIR of **1** in different solvents ($c_T = 1$ mM) showing the stretching NH and amide I bands; (b) partial ^{1}H NMR spectra of **1** recorded at different temperatures showing the aromatic and some of the aliphatic protons ($c_T = 1$ mM; CDCl$_3$; 300 MHz). The upper part of panel (b) shows the equilibrium between the free and the metastable *M** monomeric species.
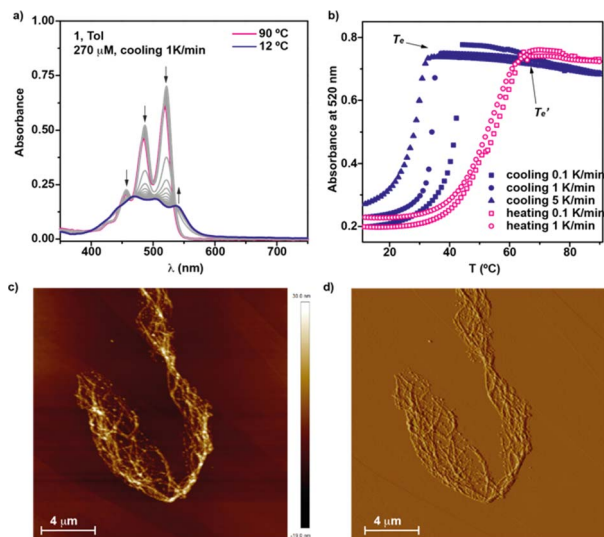
Fig. 3 (a) UV-Vis spectra of **1** in Tol at different temperatures ($c_T = 10$ M); (b) plot of the variation of the absorbance at 520 nm *versus* temperature at different cooling or heating rates; arrows in panel (a) indicate the spectral changes upon decreasing the temperature; height (c) and phase (d) AFM images of the fibrillar aggregates formed by **1** in MCH (z scale = 30 nm; $c_T = 10$ M; HOPG as surface).

diagnostic of a cooperative mechanism. However, a global fitting of these curves by applying the one-component equilibrium model yields inaccurate results, most probably due to the operation of a kinetic process provoked by the formation of the metastable monomeric species **1***M**** (Fig. 1a, b and S3†). In fact, the stability of the supramolecular polymers formed by **1** in Tol strongly depends on the cooling rate utilized to form the H-type aggregates from the monomeric species (Fig. 3b). Thus, the temperature of elongation, T_e, temperature at which the nucleation regime changes to the elongation one, decreases upon increasing the cooling rate (Fig. 3b). This effect is cancelled when the disassembly process is taken into account, *i.e.* heating a solution of the supramolecular polymers of **1** to provoke the depolymerization of **poly-1** to form the monomeric species does not show a noticeable difference in the T'_e values (Fig. 3b). Furthermore, a clear hysteresis between the cooling and heating curves is observed diagnostic of a kinetically controlled supramolecular polymerization.[13b,24] Noteworthy, during the heating and cooling processes, the absorption patterns of the involved species are identical which implies that in the kinetically controlled supramolecular polymerization of **1**, the formation of more than one aggregated species is not detected (Fig. S4†).

The stability of the supramolecular polymers formed by **1** has been quantified by performing a solvent denaturation (SD) experiment in which CHCl$_3$ and MCH are used as good and bad solvents to favor the disassembly or the aggregation, respectively. In these experiments, only monomeric and aggregated species are involved and, hence, it is possible to extract the thermodynamic parameters associated to the supramolecular polymerization of **1** by applying the SD model reported by E. W. Meijer and coworkers.[25] As expected, the addition of increasing amounts of CHCl$_3$ to the MCH solution provokes the gradual

disassembly of the aggregates species to yield the molecularly dissolved monomers (Fig. S5a†). Plotting the variation of the degree of aggregation (α) *versus* the molar fraction of the good solvent results in a quasi–sigmoidal curve that can be fitted to the SD model. This fit shed values for the Gibbs free energy of −41.9 kJ mol^{-1}, an *m* parameter, that expresses the influence of the good solvent in the disassembly process, of 27.5, and a degree of cooperativity, σ, of 0.07 (Fig. S5b†). The strong trend of BQQDI **1** to form supramolecular polymers has been visualized by atomic force microscopy (AFM) imaging. Spin-coating a diluted solution of **1** ($c_T = 10$ μM) onto highly oriented pyrolytic graphite (HOPG) shows a dense network of intertwined fibrillar structures (Fig. 3c and d).

The presence of nitrogen atoms in BQQDI **1** produces a remarkable decreasing of the LUMO level of this core in comparison to PDIs.[21] On the other hand, the molecular geometry of BQQDI **1** is similar to those of PDIs **2**.[22] The electronic and geometric features of BQQDIs make them excellent candidates to carry out copolymerization studies with PDIs **2**. Noteworthy, the aggregation mode of both PDIs **2a** and **2b** has been reported to be dissimilar. Whilst achiral **2a** self-assembles giving rise to H-type aggregates (Fig. 1b);[22] chiral **2b** affords dark-green, J-type supramolecular aggregates (Fig. 1b).[22] Furthermore, the supramolecular polymerization of **2a** has been reported to be kinetically controlled and can be accelerated by SSP.[20b] However, this is not the case of chiral **2b** that, as far as we are aware, it is not reported whether or not the J-type aggregates of **2b** are kinetically controlled and can be accelerated by SSP. Therefore, and prior to investigate the formation of the supramolecular co-polymers, we have demonstrated that chiral **2b** also follows a kinetically controlled supramolecular polymerization. Unfortunately, this PDI is scarcely soluble in Tol and we have used a mixture of MCH and 1,2-dichloroethane (DCE) in a 7/3 ratio to perform the corresponding studies for the self-assembly of **2b**. In this mixture, it is possible to achieve the absorption patterns previously reported for both the aggregated (20 °C) and the monomeric species (80 °C) of **2b** as well as a circular dichroism (CD) spectrum identical to that previously reported (Fig. S6†).[22] The cooling and heating curves of a 10 μM solution of **2b** in MCH/DCE 7/3 mixture shows a hysteresis with values of T_e and T'_e of 38 and 64 °C, respectively, that implies the trapping of the metastable M^* species between these temperatures (Fig. S7a†). These metastable M^* species evolve to the thermodynamically J-type aggregates at 39 °C upon 90 min without any lag phase (Fig. 4a). To accelerate the conversion of the M^* species of **2b** into the supramolecular polymers we have added 3% of seeds of the J-type aggregates, prepared by sonicating a 10 μM solution of **2b** in MCH/DCE 7/3 for 5 min. The addition of the seeds allows completing the conversion of the M^* monomers into the J-type aggregates in 20 min (Fig. 4a).

Similar studies have been carried out for BQQDI **1** and PDI **2a** in the same MCH/DEC 7/3 mixture. Thus, a clear hysteresis is observed for the cooling and heating curves of both dyes in this solvent mixture, thus confirming the formation of the corresponding **1***M**** and **2a***M**** species, respectively (Fig. S7b and c†). Interestingly, the kinetic evolution of the **1***M**** monomers into the corresponding H-type aggregates presents a clear lag phase
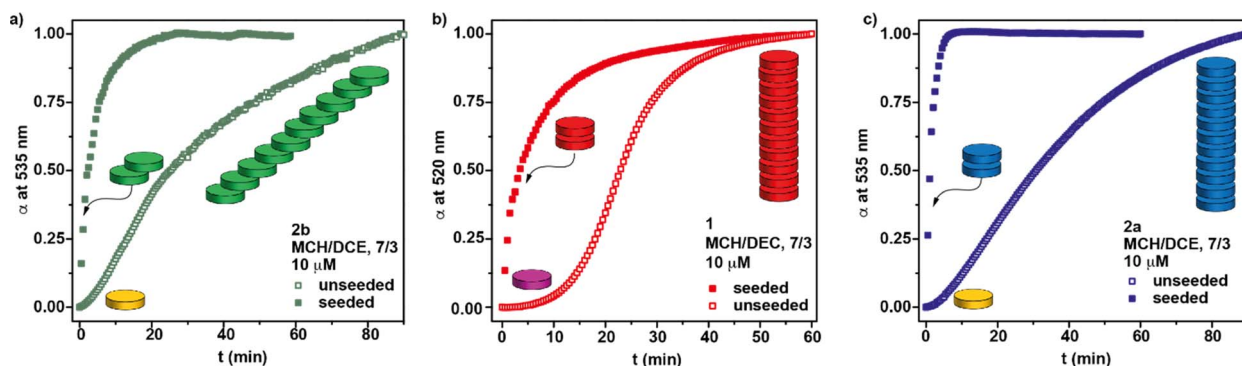
Fig. 4 Kinetic profiles of aggregate formation without and with seeds of **poly-2b** at 39 °C (a), **poly-1** at 30 °C (b); and **poly-2a** at 48 °C (c). The yellow and purple disk represents the **2M*** and **1M*** species; the green, red and blue disks represent the seeds and the homopolymers formed by **2b**, **1**, and **2a**, respectively.

ascribable to an autocatalytic process in which the full conversion into the thermodynamically controlled **poly-1** is completed upon 60 min at 30 °C (Fig. 4b). This kinetic change can be accelerated by adding seeds of **poly-1**, the completion achieved upon 30 min (Fig. 4b). The kinetic profile of **2aM*** species is very similar to those observed for **2b** and the metastable monomeric species are completely transformed into the H-type **poly-2a** species upon 90 min at 48 °C (Fig. 4c). This conversion can be accelerated by adding a 3% of seeds of these H-type aggregates and the full conversion of the **2aM*** species is completed in less than 10 min (Fig. 4c).

Seeded supramolecular polymerization and co-assembly of BQQDI 1 with PDIs 2

Upon investigating the seeded homopolymerization of all the three studied dyes **1** and **2** in the MCH/DCE 7/3 solution, we have performed a heteropolymerization study by combining the

three scaffolds. Thus, we have investigated the formation of four different supramolecular block copolymers: **poly-1-co-2a**, **poly-2a-co-1**, **poly-1-2b** and poly-2b-co-1. The schematic experimental protocol followed to prepare the kinetically controlled co-polymers is depicted in Fig. 1c.

First, we have studied the two-component seeded co-polymerization of the BQQDI **1** and the PDI **2a**, that yields H-type aggregates by the corresponding homopolymerization. To achieve co-polymer **poly-1-co-2a**, a 10 μM solution of **1** in MCH/DCE 7/3 is heated up to 80 °C to produce the complete disassembly of **poly-1** and rapidly cooled it down to 30 °C to generate kinetically trapped **1M*** species. These metastable monomers present the same absorption pattern to that observed for **1** at 80 °C, thus confirming the monomeric nature of these species (Fig. S8a†). After the addition of the seeds of PDI **2a** in a 3% ratio, the depletion of the absorption band at λ = 520 nm, ascribable to the monomeric species, was monitored. The
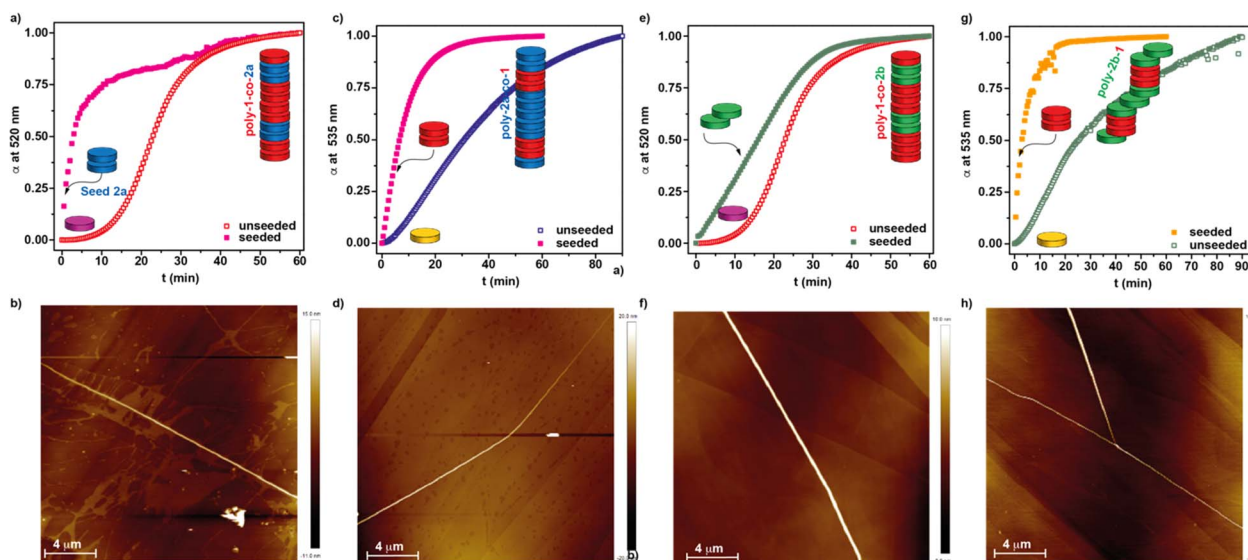

Fig. 5 Kinetic profiles (a, c, e and g) and AFM images (b, d, f and h) of kinetically controlled SSP to attain the heteropolymers **poly-1-co-2a** (a), **poly-2a-co-1** (c), **poly-1-co-2b** (e) and **poly-2b-co-1** (g). Panels (b, d, f and h) display the AFM images of the heteropolymers **poly-1-co-2a** (b), **poly-2a-co-1** (d), **poly-1-co-2b** (f) and **poly-2b-co-1** (h), respectively. The unseeded experiments in panels (a)–(d) corresponds to the polymerization of pristine homopolymers **poly-1** (red squares), **poly-2a** (blue squares) and **poly-2b** (green squares).

addition of the seeds provokes the rapid transformation of the **1M*** species into the supramolecular copolymer **poly-1-co-2a** that is completed upon 15 min (Fig. 5a).

The UV-Vis spectrum of the final **poly-1-co-2a** presents a similar pattern to that registered for pristine **poly-1**. Taking into account the stability of the fragments of **poly-2a**, acting as seeds, we can assume that the microstructure of the heteropolymer **poly-1-co-2a** would be a blocky arrangement of units with short segments of **poly-2a**, stemming from the seeds, and longer fragments of **poly-1**, corresponding to the elongated monomeric units of **1** growing from both sides of the seeds (Fig. 1c). The kinetics of both the SSP yielding the homopolymer **poly-1** and the heteropolymer **poly-1-co-2a** indicate that the rate of the conversion is not affected by the nature of the seed (Fig. 4b and 5a). The formation of the supramolecular block copolymers **poly-1-co-2a** exerts a strong influence on the morphology of the aggregates. Unlike the strongly intertwined fibrillar structures visualized for pristine **poly-1** (Fig. 3c and d), the AFM images of the heteropolymer **poly-1-co-2a** shows isolated, rod-like fibres of several micrometres in length (Fig. 5b, S9a and b†). The isolated fibres of heteropolymer **poly-1-co-2a** present uniform heights of ~12 nm all along the fibre due to the similar molecular dimensions of both BQQDI **1** and PDI **2a** (Fig. S9c†). This uniform height contrasts with the previous heteropolymers formed by planar PDI **2a** and contorted bay-substituted PDIs reported by Würthner and coworkers, in which the height of the fibre depends on the constitutive block.[20b] After attaining **poly-1-co-2a**, we have also carried out the preparation of **poly-2a-co-1** by making use of the formation of the **2M*** species and by following a similar strategy to that utilized in the previous heteropolymer. Therefore, we have heated up a solution of **2a** to 80 °C and cooled it down rapidly to 48 °C to generate the corresponding **2M*** species. After reaching this temperature, we added the seeds of **1** prepared by sonication for 5 min of a 10 μM solution of this BQQDI in a 3% ratio. The heteropolymerization yielding the H-type SBCP **poly-2a-co-1** was completed in ~30 min (Fig. 5b and S8b†). Interestingly, the SSP affording **poly-2a-co-1** is slower than the corresponding SSP homopolymerization yielding **poly-2a** which implies that the kinetics of the conversion is affected by the nature of the seed (Fig. 4c and 5c). As in the previous copolymer, the AFM images of **poly-2a-co-1** also shows the formation of long and isolated, rod-like fibres with uniform heights of ~15 nm (Fig. 5d and S9d–f†).

The previous copolymers **poly-1-co-2a** and **poly-2a-co-1** are constituted by monomeric units affording H-type aggregates upon self-assembly. In the last part of this study, we have investigated the formation of SBCPs by combining BQQDI **1** and PDI **2b** that self-assemble into H- and J-type aggregates, respectively. Heteropolymer **poly-1-co-2b** has been obtained from the metastable monomeric units **1M***, generated upon heating up a 10 μM solution of **1** in MCH/DCE 7/3 at 80 °C and rapidly cooled it down to 30 °C, and adding fragments of **poly-2b** acting as the seeds for the coassembly (Fig. 1c and 5e). The addition of the seeds of **2b** to **1M*** eliminates the lag phase observed in the kinetics of pristine **1** but slightly shortens the time at which the total conversion is completed, thus indicating

the low ability of **2b** to seed (Fig. 5e). Similarly to the above studied SBCPs, the AFM images of **poly-1-co-2b** show long fibrillar aggregates with uniform heights of ~15 nm (Fig. 5f and S9g–i†). Noteworthy, the chiral nature of the seeds of **2b** is not sufficient to induce any amplification of asymmetry effect yielding an enantioenriched helical supramolecular copolymer as demonstrates the lack of appreciable dichroic response in the CD spectrum (Fig. S10†). In addition, the UV-Vis spectrum of the final heteropolymer **poly-1-co-2b** presents the same pattern than pristine **poly-1** corresponding to the formation of H-type aggregates (Fig. S10†). Finally, we have also performed the seeded heteropolymerization of **2b**, as major component, and seeds of BQQDI **1** (Fig. 1c and 5g) by following the same strategy to that utilized for the previous heteropolymers. Thus, we prepared the metastable **2bM*** species at 39 °C and, shortly after that, we added the achiral seeds of BQQDI **1**. The formation of **poly-2b-co-1** proceeds rapidly and completed within ~15 min (Fig. 5g). In good agreement with that observed for the seeded supramolecular polymerization yielding **poly-1-co-2a** and **poly-2a-co-1**, in which seeds stemming from H-type aggregates are added, the kinetics are remarkably faster than the formation of the homopolymer **poly-2b**. Importantly, the SSP yielding **poly-2a-co-1** provokes remarkable changes in the CD spectra of this copolymer. Whilst the previously reported homopolymer **poly-2b** presents a monosignated CD signal at λ = 635 nm, diagnostic of an off-resonance coupling of transition dipoles,[26] the heteropolymer **poly-2b-co-1** exhibits a bisignated CD signal at λ = 635 nm characteristic of an on-resonance coupling of the transition dipoles characteristic of H-type aggregates (Fig. S11a†).[26] However, and despite the changes observed in the CD spectra, the absorption pattern of both pristine **poly-2b** and **poly-2b-co-1** are identical and ascribable to J-type aggregates (Fig. S11b†). These (chir)optical features can be justified by considering that the heteropolymer growth around the seeds takes place yielding columnar fragments within the whole J-type aggregate giving rise to supramolecular copolymers with a blocky microstructure (Fig. 1c).

Conclusions

Herein we report on the synthesis and self-assembling features of the 3,4,9,10-benzo[d,e]isoquinolino[1,8-g,h]quinoline-tetracarboxylic diimide (BQQDI) **1** endowed with peripheral trialkoxybenzamide fragments that favors its kinetically controlled supramolecular polymerization by the formation of intramolecularly H-bonded, seven-membered pseudocycles. The electron-withdrawing character of **1**, together with the similar geometry, makes BQQDI **1** an optimal candidate to perform seeded supramolecular copolymerization with the previously reported PDIs **2**. Thus, we have developed the synthesis of four different supramolecular block copolymers by mixing BQQDI **1** and PDIs **2**. Heteropolymers **poly-1-co-2a** and **poly-2a-co-1** are formed between two different species that separately give rise to H-type aggregates and in combination also form H-type co-assemblies. More interesting is the case of the heteropolymers formed upon mixing achiral **1** with chiral **2b** which, in turn, upon self-assembly, affords J-type aggregates.

Heteropolymer **poly-1-co-2b**, formed by seeding the metastable monomers of **1** with fragments of **2b**, presents the characteristics of H-type aggregates. However, **poly-2b-co-1**, prepared by seeding the chiral, metastable monomers of **2b** with achiral seeds of **1**, produces chiral, J-type aggregates. Interestingly, the original monosignated CD signal of pristine **poly-2b** changes to a bisignated CD signal most probably due to the formation of columnar domains around the seeds of **1**. These findings indicate the blocky nature of the supramolecular copolymers formed. The studies presented allows shedding relevant information about the formation of kinetically controlled supramolecular heteropolymers with a controlled microstructure.

Data availability

The data that supports the findings of this study have been included in the main text and ESI† and are available from the corresponding author upon reasonable request.

Author contributions

A. J. Schwalb (first author): investigation, data curation, formal analysis, visualization and revising the original draft; Dr F. García: investigation, revising the original draft, funding acquisition; Dr L. Sánchez: (corresponding author): conceptualization, supervision, validation, writing – review & editing and funding.

Conflicts of interest

There are no conflicts to declare.

Acknowledgements

Notes and references

1 (a) G. Van Meer, D. R. Voelker and G. V. Feigenson, *Nat. Rev. Mol. Cell Biol.*, 2008, **9**, 112; (b) D. Lingwood and K. Simons, *Science*, 2010, **327**, 4; (c) X. Cheng and J. C. Smith, *Chem. Rev.*, 2019, **119**, 5849.

2 (a) F. S. Bates and G. H. Fredrickson, *Phys. Today*, 1999, **52**, 32; (b) C. Sinturel, F. S. Bates, M. A. Hillmyer and N. High, *ACS Macro Lett.*, 2015, **4**, 1044; (c) H. Dau, G. R. Jones, E. Tsogtgerel, D. Nguyen, A. Keyes, Y.-S. Liu, H. Rauf, E. Ordonez, V. Puchelle, H. B. Alhan, C. Zhao and E. Harth, *Chem. Rev.*, 2022, **122**, 14471.

3 (a) T. F. A. De Greef, M. M. J. Smulders, M. Wolffs, A. P. H. J. Schenning, R. P. Sijbesma and E. W. Meijer, *Chem. Rev.*, 2009, **109**, 5687; (b) M. Wehner and F. Würthner, *Nat. Rev. Chem.*, 2020, **4**, 38.

4 Z. Álvarez, A. N. Kolberg-Edelbrock, I. R. Sasselli, J. A. Ortega, R. Qiu, Z. Syrgiannis, P. A. Mirau, F. Chen, S. M. Chin, S. Weigand, E. Kiskinis and S. I. Stupp, *Science*, 2021, **374**, 848.

5 R. P. Sijbesma, F. H. Beijer, L. Brunsveld, B. J. B. Folmer, K. J. H. K. Hirschberg, R. F. M. Lange, J. K. L. Lowe and E. W. Meijer, *Science*, 1997, **278**, 1601.

6 O. Dumele, L. Đorđević, H. Sai, T. J. Cotey, M. H. Sangji, K. Sato, A. J. Dannenhoffer and S. I. Stupp, *J. Am. Chem. Soc.*, 2022, **144**, 3127.

7 W. Zhao, J. Tropp, B. Qiao, M. Pink, J. D. Azoulay and A. H. Flood, *J. Am. Chem. Soc.*, 2020, **142**, 2579.

8 Y. Yanagisawa, Y. Nan, K. Okuro and T. Aida, *Science*, 2018, **359**, 72.

9 (a) Y. Yamamoto, T. Fukushima, Y. Suna, N. Ishii, A. Saeki, S. Seki, S. Tagawa, M. Taniguchi, T. Kawai and T. Aida, *Science*, 2006, **314**, 1761; (b) R. Rodríguez, C. Naranjo, A. Kumar, P. Matozzo, T. Kumar Das, Q. Zhu, N. Vanthuyne, R. Gómez, R. Naaman, L. Sánchez and J. Crassous, *J. Am. Chem. Soc.*, 2022, **144**, 7709.

10 H. M. M. ten Eikelder and A. J. Markvoort, *Acc. Chem. Res.*, 2019, **52**, 3465.

11 J. Matern, Y. Dorca, L. Sánchez and G. Fernández, *Angew. Chem., Int. Ed.*, 2019, **58**, 16730.

12 J. B. Gilroy, T. Gädt, G. R. Whittell, L. Chabanne, J. M. Mitchels, R. M. Richardson, M. A. Winnik and I. Manners, *Nat. Chem.*, 2010, **2**, 566.

13 (a) S. Ogi, K. Sugiyasu, S. Manna, S. Samitsu and M. Takeuchi, *Nat. Chem.*, 2014, **6**, 188; (b) J. Kang, D. Mijayima, T. Mori, Y. Inoue, Y. Itoh and T. Aida, *Science*, 2015, **347**, 646; (c) S. Ogi, V. Stepanenko, K. Sugiyasu, M. Takeuchi and F. Würthner, *J. Am. Chem. Soc.*, 2015, **137**, 3300.

14 B. Adelizzi, N. J. Van Zee, L. N. J. de Windt, A. R. A. Palmans and E. W. Meijer, *J. Am. Chem. Soc.*, 2019, **141**, 6110.

15 H. M. M. ten Eikelder, B. Adelizzi, A. R. A. Palmans and A. J. Markvoort, *J. Phys. Chem. B*, 2019, **123**, 6627.

16 (a) B. Adelizzi, P. Chidchob, N. Tanaka, B. G. A. Lamers, S. C. J. Meskers, S. Ogi, A. R. A. Palmans, S. Yamaguchi and E. W. Meijer, *J. Am. Chem. Soc.*, 2020, **142**, 16681; (b) H. Su, S. A. H. Jansen, T. Schnitzer, E. Weyandt, A. T. Rösch, J. Liu, G. Vantomme and E. W. Meijer, *J. Am. Chem. Soc.*, 2021, **143**, 17128; (c) R. Liao, F. Wang, Y. Guo, Y. Han and F. Wang, *J. Am. Chem. Soc.*, 2022, **144**, 9775; (d) L. López-Gandul, A. Morón-Blanco, F. García and L. Sánchez, *Angew. Chem., Int. Ed.*, 2023, **62**, e202308749.

17 S. H. Jung, D. Bochicchio, G. M. Pavan, M. Takeuchi and K. A. Sugiyasu, *J. Am. Chem. Soc.*, 2018, **140**, 10570.

18 S. Sarkar, A. Sarkar, A. Som, S. S. Agasti and S. J. George, *J. Am. Chem. Soc.*, 2021, **143**, 11777.

19 F. Würthner, C. R. Saha-Möller, B. Fimmel, S. Ogi, P. Leowanawat and D. Schmidt, *Chem. Rev.*, 2016, **116**, 962.

20 (a) D. Görl, X. Zhang, V. Stepanenko and F. Würthner, *Nat. Commun.*, 2015, **6**, 7009; (b) W. Wagner, M. Wehner, V. Stepanenko and F. Würthner, *J. Am. Chem. Soc.*, 2019, **141**, 12044.

21 (a) T. Okamoto, S. Kumagai, E. Fukuzaki, H. Ishii, G. Watanabe, N. Niitsu, T. Annaka, M. Yamagishi, Y. Tani, H. Sugiura, T. Watanabe, S. Watanabe and J. Takeya, *Sci.*

Adv., 2020, **6**, eaaz0632; (*b*) S. Kumagai, H. Ishii, G. Watanabe, C. P. Yu, S. Watanabe, J. Takeya and T. Okamoto, *Acc. Chem. Res.*, 2022, **55**, 660.

22 (*a*) S. Ghosh, X.-Q. Li, V. Stepanenko and F. Würthner, *Chem.–Eur. J.*, 2008, **14**, 11343; (*b*) F. Würthner, C. Bauer, V. Stepanenko and S. Yagai, *Adv. Mater.*, 2008, **20**, 1695; (*c*) W. Wagner, M. Wehner, V. Stepanenko and F. Würthner, *J. Am. Chem. Soc.*, 2019, **141**, 12044.

23 (*a*) M. Wehner, M. I. S. Röhr, M. Böhler, V. Stepanenko, W. Wagner and F. Würthner, *J. Am. Chem. Soc.*, 2019, **141**, 6092; (*b*) C. Naranjo, S. Adalid, R. Gómez and L. Sánchez, *Angew. Chem., Int. Ed.*, 2023, **62**, e202218572.

24 (*a*) E. E. Greciano and L. Sánchez, *Chem.–Eur. J.*, 2016, **22**, 13724; (*b*) E. E. Greciano, J. Calbo, E. Ortí and L. Sánchez, *Angew. Chem., Int. Ed.*, 2020, **59**, 17517; (*c*) E. E. Greciano, S. Alsina, G. Ghosh, G. Fernández and L. Sánchez, *Small Methods*, 2020, **4**, 1900715.

25 (*a*) P. A. Korevaar, C. Schaefer, T. F. A. de Greef and E. W. Meijer, *J. Am. Chem. Soc.*, 2012, **134**, 13482; (*b*) L. López-Gandul, C. Naranjo, C. Sánchez, R. Rodríguez, R. Gómez, J. Crassous and L. Sánchez, *Chem. Sci.*, 2022, **13**, 11577.

26 N. S. S. Nizar, M. Sujith, K. Swathi, C. Sissa, A. Painelli and K. G. Thomas, *Chem. Soc. Rev.*, 2021, **50**, 11208.